Available online at www.sciencedirect.com
ScienceDirect
Journal of Nuclear Materials 357 (2006) 48–57
journal of nuclear materials
www.elsevier.com/locate/jnucmat

Thermodynamic assessment of the LiF–BeF_2–ThF_4–UF_4 system

J.P.M. van der Meer [a], R.J.M. Konings [a,*], H.A.J. Oonk [b]

[a] European Commission, Joint Research Centre, Institute for Transuranium Elements, P.O. Box 2340, 76125 Karlsruhe, Germany
[b] Petrology Group, Faculty of Geosciences, Utrecht University, Budapestlaan 4, 3584 CD Utrecht, Netherlands

Received 23 March 2006; accepted 23 May 2006

Abstract

The liquid phases of the LiF–BeF_2–ThF_4–UF_4 binary subsystems have been assessed using a quasi-chemical model with general polynomial description. By extrapolating the optimized Gibbs energy terms from the binaries, the ternary subsystems were calculated, which form the boundaries of the quaternary system. A good agreement with experimental data on the ternary systems was obtained.

1. Introduction

The Molten Salt Reactor (MSR) is one of the innovative nuclear reactor systems of the Generation IV programme. The concept of this reactor, in which the fuel is dissolved in a circulating molten fluoride salt mixture, was already developed in the 1960s in Oak Ridge National Laboratory, USA. The knowledge acquired in that period forms a base for the current MSR designs. The MSR has the capability of breeding of uranium from thorium in a thermal spectrum, where neutron capture of ^{232}Th forms ^{233}Pa, which decays to ^{233}U, a fissile isotope. Not the best neutronic conditions facilitating this reaction, but also other thermal and physicochemical requirements have to be met. It has been demonstrated that LiF–BeF_2 is the most appropriate solvent for the fuels, where LiF needs to be enriched in ^{7}LiF because of neutronic considerations. A small percentage of a fissile isotope, usually ^{235}U, is needed to start the neutron capture reaction. A typical fuel composition for the MSR is therefore a LiF–BeF_2–ThF_4–UF_4 mixture.

Extensive experimental research has been carried out on the LiF–BeF_2 phase diagrams [1–6], which we have assessed in a previous paper [7]. One of our main findings was the existence of a miscibility gap in LiF–BeF_2, which was also predicted in the ternary system LiF–BeF_2–ThF_4, in contrast to the conclusions from experimental studies by ORNL researchers [8] on this system. This paper deals with the extension of the thermodynamic assessment to the quaternary system LiF–BeF_2–ThF_4–UF_4. All binary subsystems were assessed according to the CALPHAD method, from which the four ternaries were derived. The results were compared to the experimental data for LiF–BeF_2–UF_4 [9], LiF–ThF_4–UF_4 [10] and BeF_2–ThF_4–UF_4 [11].

* Corresponding author. Tel.: +49 7247 951391; fax: +49 7247 951566.
E-mail address: rudy.konings@ec.europa.eu (R.J.M. Konings).

0022-3115/$ - see front matter © 2006 Elsevier B.V. All rights reserved.
doi:10.1016/j.jnucmat.2006.05.042

2. Thermodynamic assessment

2.1. Calculation of the binary phase diagrams

Gibbs energy functions of all phases of the system, including the excess Gibbs energy coefficients of the solution phase(s) present, are necessary to describe a T–X phase diagram. When they are unknown, they can be obtained by performing a thermodynamic assessment. The missing coefficients in the Gibbs energy as well as in the excess equations are optimized so that a best fit is found between the known Gibbs energy functions of the phases and the available experimental data.

The Gibbs energy functions for the relevant compounds are set up after careful investigation of thermodynamic tables [12] in such a way that they are described as the polynomial in Eq. (1).

$$G(T) = a + bT + cT\ln(T) + \sum d_i T^i. \quad (1)$$

The thermodynamic data for the compounds LiF, BeF_2, $LiF \cdot BeF_2$, ThF_4 and UF_4 were taken from an internal report [13]. This was not the case for the large number of intermediate compounds present in this system. Their Gibbs energy equations were obtained by optimizations which were done using the OptiSage module in the FactSage 5.3 software package [14]. It should be noted that the G functions can normally be split into $\Delta_f H^0$, S^0 and C_p functions. However, without any calorimetric evidence for the intermediate compounds, assigning a value to $\Delta_f H^0$ and S^0 could and should not be done. It has therefore been chosen to give the G functions instead. Table 1 lists these parameters, the literature data as well as the assessed values.

The model used to describe the excess Gibbs energy of the solution phase, was the quasi-chemical model by Pelton and Blander [15]. This treats a binary system in which symmetry group numbers i and j are attributed to the components A and B, allowing 'i' and 'j' particles to mix substitutionally on a quasi-lattice. In this formalism, general polynomials can be used to describe the excess Gibbs energy coefficients. The equation for a binary system $A - B$ is given in Eq. (2).

$$\Delta_{xs}G = \sum_{p,q} L^{p,q}_{A,B}(T) Y_A \left(\frac{\chi_i}{\chi_i + \chi_j}\right)^p Y_B \left(\frac{\chi_j}{\chi_i + \chi_j}\right)^q. \quad (2)$$

$L^{p,q}_{A,B}(T)$ is the excess Gibbs energy term as a function of temperature. In this case, a linear dependence $L_{A,B}(T) = {}^kL_{A,B} + {}^lL_{A,B} \times T$ was chosen. Y_A and Y_B are the equivalent fractions of the components, p and q are the power coefficients of the equivalent fraction expression, while χ_i and χ_j are

Table 1
Gibbs energy functions for the pure components and intermediate compounds of the system LiF–BeF_2–ThF_4–UF_4, valid in the temperature range of 298–1500 K

Compound	a	bT	$cT\ln T$	dT^2	e/T
LiF (l)[a]	−6.177902E+05	3.86910E+02	−6.4183E+01	−2.2468E−02	
BeF_2 (l)[a]	−1.035874E+06	2.27400E+02	−4.0984E+01		
ThF_4 (l)[a]	−2.104414E+06	7.40179E+02	−1.3390E+02		
UF_4 (l)[a]	−1.966757E+06	1.05494E+03	−1.7474E+02		
LiF (cr)[a,b]	−6.324819E+05	2.62493E+02	−4.3309E+01	−8.1561E−03	2.84562E+05
BeF_2 (cr,α)[c]	−1.037387E+06	1.07771E+02	−1.9181E+01	−5.4769E−02	
BeF_2 (cr,β)[c]	−1.039380E+06	2.21961E+02	−3.9457E+01	−2.3128E−02	
ThF_4 (cr)[a]	−2.138907E+06	6.85770E+02	−1.2217E+02	−4.1850E−03	6.27500E+05
UF_4 (cr)[a]	−1.950643E+06	6.23757E+02	−1.1452E+02	−1.0277E−02	2.06580E+05
Li_2BeF_4 (cr)[d]	−2.307288E+06	5.21881E+02	−9.0779E+01	−7.4575E−02	−9.85416E+04
Li_4UF_8 (cr)[e]	−4.460463E+06	1.61734E+03	−2.8672E+02	−4.4921E−02	1.34364E+06
$LiUF_5$ (cr)[e]	−2.605258E+06	8.90824E+02	−1.5757E+02	−1.8938E−02	4.90845E+05
LiU_4F_{17} (cr)[e]	−8.528884E+06	2.82132E+03	−5.0113E+02	−4.9771E−02	1.11058E+06
Li_3ThF_7 (cr)[e]	−4.126070E+06	1.54095E+03	−2.5133E+02	−3.0167E−02	1.48030E+06
$LiThF_5$ (cr)[e]	−2.869220E+06	1.03581E+03	−1.6522E+02	−1.2846E−02	9.11765E+05
$LiTh_2F_9$ (cr)[e]	−5.026788E+06	1.72295E+03	−2.8740E+02	−1.7031E−02	1.53927E+06
$LiTh_4F_{17}$ (cr)[e]	−9.335026E+06	3.11328E+03	−5.3174E+02	−2.5401E−02	2.79427E+06

[a] Data taken from Ref. [13].
[b] A small, but significant extra term was needed for a satisfactory description of the G function: $-8.4117E{-}08 \cdot T^3$.
[c] A transition from low quartz to high quartz occurs at 500 K.
[d] Idem as for[b]: a small extra term was necessary: $3.0693E{-}09 \cdot T^3$.
[e] Obtained by assessment with the general polynomial model.

the sum of the equivalent fractions in the same symmetry group with i and j as indices for the group numbers. It is possible to rewrite the Redlich–Kister equation for binary interactions in the general polynomial notation if the equivalent fractions are similar to the mole fractions. The optimized values for the binaries of LiF–BeF_2–ThF_4–UF_4 can be found in Table 2. The optimization of complex systems with a number of intermediate compounds, of which the thermodynamic data needed to be optimized as well, led to high excess values in order to obtain a satisfying description of the diagram. It should be noted that the ${}^{k}L_{A,B}$ and ${}^{l}L_{A,B}$ terms are mathematical parameters and cannot automatically be translated to parameters with a physical meaning, namely an excess enthalpy and entropy.

2.2. Calculation of higher order phase diagrams

The ternary phase diagrams were obtained by extrapolation of the binary interaction coefficients. The Kohler–Toop method was applied, which is suitable for chemically asymmetric systems. In the systems LiF–ThF_4–UF_4 and BeF_2–ThF_4–UF_4, the chemical asymmetric component is evidently LiF and BeF_2, respectively. However, for LiF–BeF_2–ThF_4 and LiF–BeF_2–UF_4 discussion could arise how to treat the different components. In this case, LiF was selected as the asymmetrical component, as will be explained below.

Table 2
Optimized excess Gibbs parameters of the liquid phase for the binaries of LiF–BeF_2–ThF_4–UF_4, valid to at least 1500 K

A, B	p	q	${}^{k}L_{A,B}$/J mol^{-1}	${}^{l}L_{A,B}$/J K^{-1} mol^{-1}
UF_4–LiF	0	0	−75.252	−25.837
	0	1	−78694	38.406
ThF_4–LiF	0	0	−141298	102.50
	1	0	43130	−29.459
	0	1	−52637	38.821
BeF_2–LiF	0	0	−15580	−11.645
	1	0	71320	−63.487
	0	1	−71320	63.487
	1	1	−9612.0	0.000
	2	1	4806.0	0.000
	1	2	4806.0	0.000
UF_4–BeF_2	0	0	−33606	9.985
	1	0	−1630.0	27.447
	0	1	68012	−27.462
ThF_4–BeF_2	0	0	16749	−11.462
UF_4–ThF_4[a]	0	0	661.46	−1.4789

[a] ThF_4 and UF_4 form a solid solution.

3. Results and discussion

3.1. The binary subsystems of LiF–BeF_2–ThF_4–UF_4

Six binary subsystems are needed to build the four ternaries which represent the quaternary LiF–BeF_2–ThF_4–UF_4 system. LiF–BeF_2, LiF–ThF_4 and BeF_2–ThF_4 have been described in a previous publication [7]. The assessed diagrams reproduce the experimental results well, except for the LiF–BeF_2 system. Here the assessment mandates the existence of a small miscibility gap near to the BeF_2 boundary, in order to obtain an agreement between the enthalpy of fusion of BeF_2 and the experimental liquidus data. LiF–UF_4 is the most complex diagram, containing a number of intermediate components: $4LiF \cdot UF_4$, $LiF \cdot UF_4$ and $LiF \cdot 4UF_4$. The assessed diagram of LiF–UF_4 is shown in Fig. 1. Similar is the diagram of LiF–ThF_4, which was published in [7], but is shown here again for clarity in Fig. 2. BeF_2–UF_4 is a simple

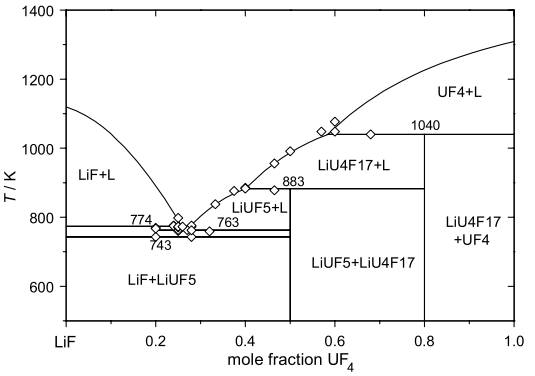

Fig. 1. Assessed LiF–UF_4 diagram, (◇) experimental data by Thoma et al. [21].

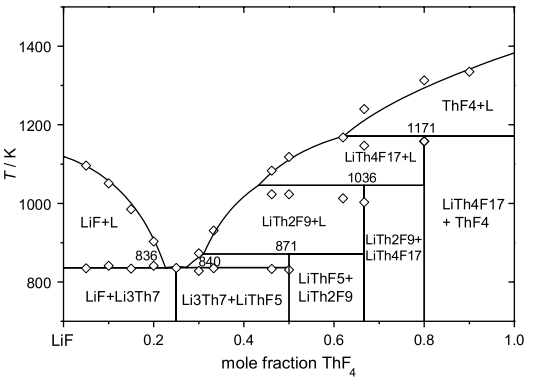

Fig. 2. Assessed LiF–ThF_4 diagram, (◇) experimental data by Thoma et al. [21].

eutectic system with the eutectic point close to the BeF_2 axis. The assessed diagram is shown in Fig. 3. ThF_4–UF_4 form a continuous solid solution series without a temperature minimum; the experimental data, consisting of four points, are very limited. Fig. 4 shows the diagram. Data on the binaries can be found in Table 3.

3.2. *LiF–BeF_2–ThF_4–UF_4 and the ternary subsystems*

Fig. 5 shows the calculated liquidus surfaces of LiF–BeF_2–ThF_4, LiF–BeF_2–UF_4, LiF–ThF_4–UF_4 and BeF_2–ThF_4–UF_4, such that they form a quaternary system. The figure can be considered as an open-folded tetrahedron with LiF–BeF_2–ThF_4 as the base and UF_4 at the apex.

LiF–BeF_2–ThF_4 contains a eutectic and a (quasi)-peritectic point in the LiF rich part. Another eutectic (695.0 K) and a quasi-peritectic (751.0 K)

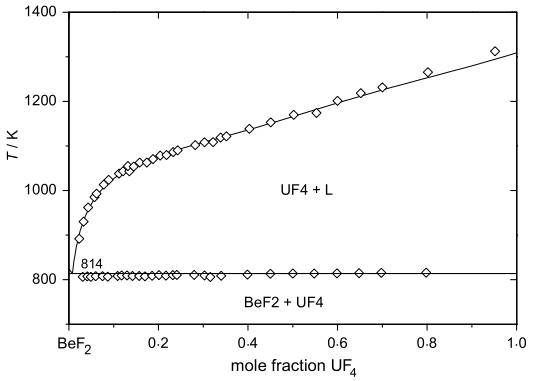

Fig. 3. Assessed BeF_2–UF_4 diagram, (◇) experimental data by Jones et al. [9].

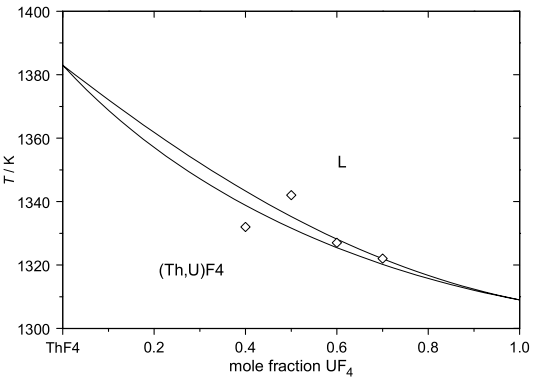

Fig. 4. Assessed ThF_4–UF_4 diagram, (◇) experimental data by Weaver et al. [10].

Table 3
Invariant equilibria in the binary subsystems of LiF–BeF_2–ThF_4–UF_4, calculated and *experimental* (*in italics*)[a]

System *A–B*	X_B	T/K	$X_{B,exp}$	T_{exp}/K	Type invariant
LiF–UF_4[a]	0.200	742.8	*0.200*	*743*	Lower stab. $4LiF \cdot UF_4$
	0.258	774.2	*0.26*	*773*	Peritectic
	0.269	763.7	*0.27*	*763*	Eutectic
	0.400	883.1	*0.40*	*883*	Peritectic
	0.586	1040.0	*0.57*	*1048*	Peritectic
LiF–ThF_4[b]	0.224	836.4	*0.23*	*841*	Eutectic
	0.250	846.5	*0.25*	*846*	Congr. m.p.
	0.283	840.0	*0.29*	*838*	Eutectic
	0.302	871.2	*0.305*	*870*	Peritectic
	0.428	1035.7	*0.42*	*1035*	Peritectic
	0.603	1171.2	*0.62*	*1170*	Peritectic
LiF–BeF_2[c]	0.330	728.6	*0.328*	*732.0*	Eutectic
	0.333	728.7	*0.333*	*732.3*	Congr. m.p.
	0.519	635.0	*0.531*	*636.7*	Eutectic
	0.760	786.5	*Not found*		Begin RoD[f]
	0.871	811.9			Max. RoD
	0.950	786.5			End RoD
BeF_2–UF_4[d]	0.008	813.6	*0.005*	*808*	Eutectic
BeF_2–ThF_4[e]	0.023	794.8	*0.020*	*800*	Eutectic

[a] Experimentally determined invariant points by Barton et al. [22].
[b] By Thoma et al. [21].
[c] By Romberger et al. [6].
[d] By Jones et al. [9].
[e] By Thoma et al. [8].
[f] Region of demixing.

are found very near to the LiF–BeF_2 axis, which is indicated in Table 4. The assessed diagram of LiF–BeF_2–ThF_4 was published previously [7]. However, in the present paper a modification of the diagram is shown. The diagram we published first [7] was characterized by a significant ternary miscibility gap in the BeF_2 apex. A more thorough discussion can be found in Section 3.5.

LiF–BeF_2–UF_4 is analogous to the former system, but not similar, as LiF–UF_4 has one intermediate compound less than LiF–ThF_4. The point, at which $LiF \cdot 4UF_4$ decomposes, is very near to the LiF–UF_4 axis of the ternary. A eutectic can be found in the LiF rich region (712.9 K). Two other invariant points, a quasi-peritectic (691.9 K) and eutectic (695.0 K), nearly touch the LiF–BeF_2 axis.

LiF–ThF_4–UF_4 contains three solid solution series: $LiF \cdot (Th,U)F_4$, $LiF \cdot 4(Th,U)F_4$ and $(Th,U)F_4$. The solid–liquid phase diagram of ThF_4–UF_4 (Fig. 4) shows evidence of weak deviations from ideal-mixing behavior. For that matter, the solid solutions were treated as ideal mixtures, putting all deviations from ideality in the liquid. One eutectic

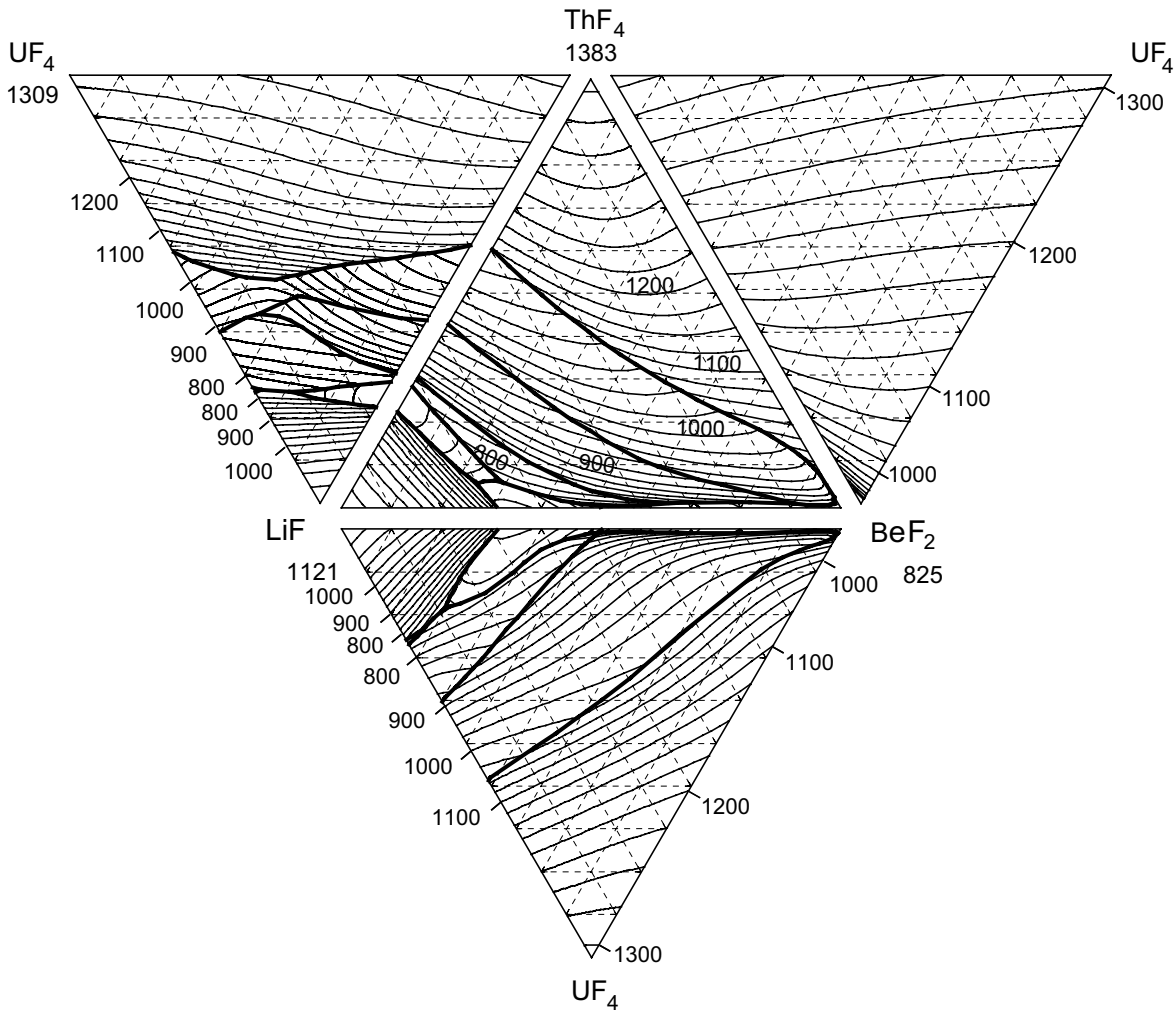

Fig. 5. Calculated liquidus surface of LiF–BeF_2–ThF_4, LiF–BeF_2–UF_4, LiF–ThF_4–UF_4 and BeF_2–ThF_4–UF_4, combined to a quaternary system. Melting temperatures are labelled in K and isotherms with an interval of 25 K are shown.

(760.2 K) and two quasi-peritectic points (767.7 and 903.8 K) are present in this ternary. The invariant points of the three ternary systems mentioned above are described in Table 4.

The simplest of the four ternaries is BeF_2–ThF_4–UF_4, where the solid solution series between ThF_4 and UF_4 dominates. A ternary eutectic point does not exist, however, but the two binary eutectics are connected close to the BeF_2 apex.

3.3. Comparison ternary model and experimental data

Table 4 lists the invariant points of the systems LiF–BeF_2–ThF_4, LiF–BeF_2–UF_4 and LiF–ThF_4–UF_4, as found in the calculated diagrams and compares these to the experimentally derived values. It can be noticed that many calculated equilibria differ, not only in temperature, but also in composition, from the experimental ones. The composition of a ternary invariant point is sometimes not so straightforward as one would expect from studying the ternary diagram. When plotting binary cross-sections, the so-called pseudobinaries, far more complicated phase field relationships are revealed, which are not directly visible in the ternary.

Tables belonging to the papers [8–10], which were deposited at the Library of Congress in Washington DC, contained all experimental data on LiF–BeF_2–ThF_4 (thermal gradient quenching and DTA cooling), LiF–BeF_2–UF_4 (DTA cooling, thermal gradient quenching and high-temperature filtration)

Table 4
Invariant equilibria in the ternary subsystems *A–B–C* of LiF–BeF_2–ThF_4–UF_4, calculated and *experimental* (*in italics*)[a]

A LiF	*B* BeF_2	*C* ThF_4	*T*/K	Type invariant	Phases present
0.70	0.24	0.06	758.9	Eutectic[b]	$LiF + 3LiF \cdot ThF_4 + 2LiF \cdot BeF_2 = L$
0.65	0.29	0.06	754.7	Peritectic	$3LiF \cdot ThF_4 + LiF \cdot ThF_4 + 2LiF \cdot BeF_2 + L$[c]
0.48	0.515	0.005	695.0	Eutectic	$2LiF \cdot BeF_2 + BeF_2 + LiF \cdot ThF_4 = L$
0.34	0.65	0.01	751.0	Peritectic	$LiF \cdot ThF_4 + LiF \cdot 2ThF_4 + BeF_2 + L$[d]
0.66	*0.30*	*0.04*	*717*	*Peritectic*	$LiF + 3LiF \cdot ThF_4 + 2LiF \cdot BeF_2 + L$
0.63	*0.30*	*0.07*	*721*	*Peritectic*	$3LiF \cdot ThF_4 + LiF \cdot ThF_4 + LiF \cdot 2ThF_4 + L$
0.61	*0.36*	*0.03*	*706*	*Peritectic*	$3LiF \cdot ThF_4 + LiF \cdot 2ThF_4 + 2LiF \cdot BeF_2 + L$
0.47	*0.51*	*0.02*	*629*	*Eutectic*	$2LiF \cdot BeF_2 + BeF_2 + LiF \cdot 2ThF_4 + L$
0.34	*0.64*	*0.03*	*728*	*Peritectic*	$LiF \cdot 2ThF_4 + LiF \cdot 4ThF_4 + BeF_2 + L$
0.15	*0.83*	*0.02*	*770*	*Peritectic*[f]	$ThF_4 + LiF \cdot 4ThF_4 + BeF_2 + L$
LiF	BeF_2	UF_4			
0.72	0.05	0.23	742.3		Decomposition of $4LiF \cdot UF_4$
0.70	0.12	0.18	712.9	Eutectic	$LiF + LiF \cdot UF_4 + 2LiF \cdot BeF_2 = L$
0.49	0.50	0.01	695.0	Eutectic	$2LiF \cdot BeF_2 + LiF \cdot UF_4 + BeF_2 = L$
0.48	0.51	0.01	691.9	Peritectic	$2LiF \cdot BeF_2 + LiF \cdot 4UF_4 + BeF_2 + L$[e]
0.72	*0.06*	*0.22*	*753*	*Peritectic*	*Decomposition of* $4LiF \cdot UF_4$
0.69	*0.23*	*0.08*	*699*	*Eutectic*	$LiF + LiF \cdot UF_4 + 2LiF \cdot BeF_2 + L$
0.48	*0.515*	*0.005*	*623*	*Eutectic*	$2LiF \cdot BeF_2 + LiF \cdot UF_4 + LiF \cdot 4UF_4 + L$
0.455	*0.54*	*0.005*	*654*	*Peritectic*	$2LiF \cdot BeF_2 + LiF \cdot 4UF_4 + BeF_2 + L$
0.295	*0.70*	*0.005*	*756*	*Peritectic*[f]	$UF_4 + LiF \cdot 4UF_4 + BeF_2 + L$
LiF	ThF_4	UF_4			
0.74	0.07	0.19	767.7	Peritectic	$LiF + LiF \cdot (Th,U)F_4 + L$[g]
0.735	0.015	0.25	760.2	Eutectic	$LiF + 4LiF \cdot UF_4 + LiF \cdot (Th,U)F_4 = L$
0.56	0.10	0.34	903.8	Peritectic	$LiF \cdot (Th,U)F_4 + LiF \cdot 4(Th,U)F_4 + L$[h]
0.725	*0.07*	*0.205*	*773*	*Peritectic*	$LiF + 3LiF \cdot ThF_4 + 4LiF \cdot UF_4$
0.72	*0.015*	*0.265*	*761*	*Eutectic*	$LiF + 4LiF \cdot UF_4 + LiF \cdot (Th,U)F_4 + L$
0.63	*0.18*	*0.19*	*882*	*Peritectic*	$LiF \cdot (Th,U)F_4 + LiF \cdot 2ThF_4 + LiF \cdot 4(Th,U)F_4 + L$

[a] Values in *italics* are proposed values, based on experiments and extrapolation. LiF–BeF_2–ThF_4 was analyzed by Thoma et al. [8], LiF–BeF_2–UF_4 by Jones et al. [9] and LiF–ThF_4–UF_4 by Weaver et al. [10].

[b] $2LiF \cdot BeF_2$ was considered as incongruently melting compound at the time of analysis. However, detailed measurements by Romberger et al. [6] showed that it melts congruently, so that the peritectic can now be interpreted as eutectic point.

[c] Saddle point: $3LiF \cdot ThF_4 + LiF \cdot ThF_4 + 2LiF \cdot BeF_2 + L = 2LiF \cdot BeF_2 + L$.

[d] Saddle point: $LiF \cdot ThF_4 + LiF \cdot 2ThF_4 + BeF_2 + L = L$.

[e] Saddle point: $2LiF \cdot BeF_2 + LiF \cdot 4UF_4 + BeF_2 = 2LiF \cdot BeF_2 + L$.

[f] This peritectic point has not been found in the calculated diagram.

[g] Saddle point: $LiF + LiF \cdot (Th,U)F_4 + L = L$.

[h] Saddle point: $LiF \cdot (Th,U)F_4 + LiF \cdot 4(Th,U)F_4 + L = L$.

and LiF–ThF_4–UF_4 (thermal gradient quenching). A comparison was made between liquidus surface of the calculated and the experimentally defined diagrams. Therefore, all liquidus data were carefully extracted from the data tables. Then the precipitation temperature of these compositions were calculated using the Equilib module in FactSage. The difference between model and experimental temperature was normalized by the experimental temperature T_{exp} and plotted versus T_{exp}. The results are shown in Fig. 6. It can be seen that the agreement in all three systems is generally good, all within ±10%, while 79.1% of the data agree better than ±5%. It must be noted, however, that the difference between the quenching and the cooling results is significant. A comparison was made between liquidus temperatures obtained by cooling and those obtained by quenching for similar compositions. It appeared that differences from 20, 30, even up to 70 K are common. Thus, as the data scatter internally to this extent, it makes it complicated to determine the differences between the model and experiment. Performing our own DTA experiments would be priority in a future study on this system.

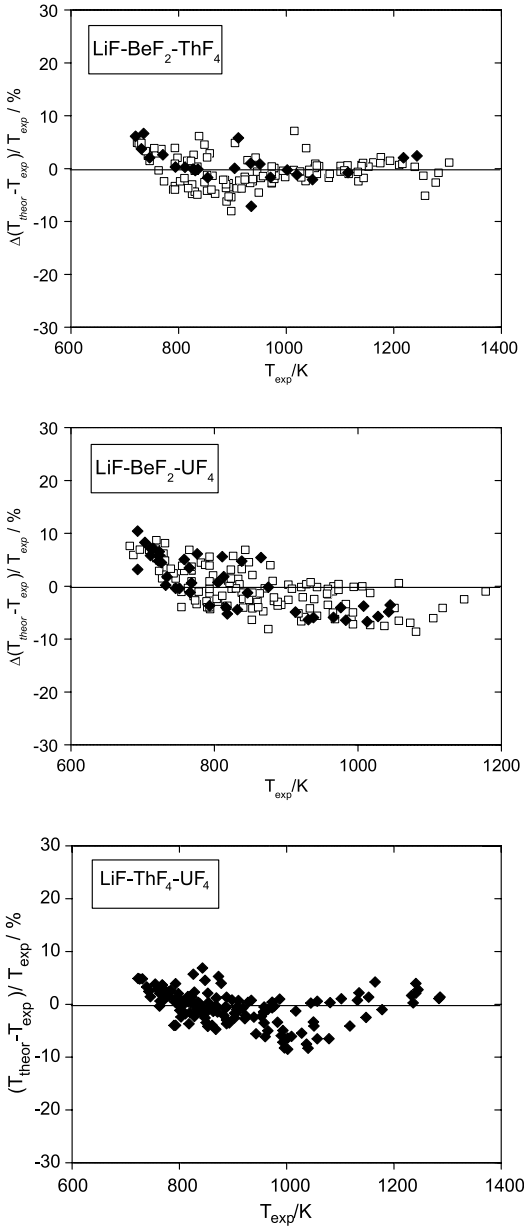

Fig. 6. Difference between the calculated and the experimental ternary liquidus temperature T_{exp} of LiF–BeF_2–ThF_4, LiF–BeF_2–UF_4 and LiF–ThF_4–UF_4, normalized by T_{exp}, versus T_{exp}. Open symbols: obtained by cooling; closed symbols: obtained by quenching.

3.4. Comparison quaternary model and experimental data

A comparison considering the possible composition for a molten salt reactor was also made. The Molten Salt Breeder Reactor, MSBR, was designed in the 1960s to breed ^{233}U from ^{232}Th in a LiF–BeF_2 melt. A favorable composition was 71.7% LiF–16% BeF_2–12% ThF_4–0.3% UF_4 in moles, with the small amount of UF_4 to start the reaction [16]. The temperature of first fusion was derived to be (773 ± 5) K, according to a report by Cantor [17]. This is in reasonable agreement with the somewhat higher calculated temperature of 794.5 K, which is the precipitation temperature of the composition 71.7% LiF–16% BeF_2–12.3% $(Th_{0.9756}U_{0.0244})F_4$. It has been found as well that without the addition of 0.3% UF_4 the precipitation temperature would increase by exactly 2 K. Four possible compositions for breeder fuel, which were analyzed by Cantor [17], appear in Table 5 with the experimentally determined and calculated temperatures.

Table 5
Compositions of MSR breeder fuel as proposed by ORNL with experimental and calculated temperature

LiF	BeF_2	ThF_4	UF_4	T_{exp}/K	T_{cal}/K
0.73	0.16	0.107	0.003	773	790
0.72	0.21	0.067	0.003	773	794
0.68	0.20	0.117	0.003	753	785
0.63	0.25	0.117	0.003	773	790

3.5. LiF–BeF_2–ThF_4 reassessed

As was stated above, the diagram of LiF–BeF_2–ThF_4 shown here is different from the one published by us previously [7], which contains a significant miscibility gap in the BeF_2 corner. This was the result of a model assuming that BeF_2 was the chemically asymmetric component in LiF–BeF_2–ThF_4, which was given therefore a different weight in the Kohler–Toop extrapolation of the binary excess Gibbs coefficients. BeF_2 was selected because it is known to form polymeric species in the liquid phase and it was therefore anticipated to exert a different behavior than the other two compounds. However, we realized after comparing the excess Gibbs energy curves of the three binaries that selecting LiF would be a better option.

As it can be seen in Fig. 7, the excess Gibbs curves of LiF–BeF_2 and LiF–ThF_4 at 1100 K are both negative and of the same order of magnitude. This is in contrast to the BeF_2–ThF_4 curve, which is smaller and positive at the same temperature. This difference due to the presence of LiF could be explained by the fact that LiF is highly ionic, whereas BeF_2 and ThF_4 have the tendency to form more molecular-type ions as BeF_4^{2-} [18] and ThF_6^{2-} in the melt. Raman spectroscopy on molten LiF–

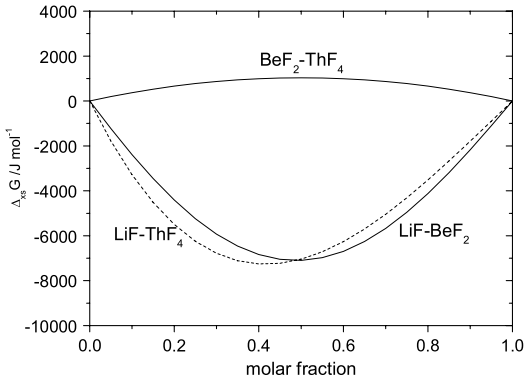

Fig. 7. Excess Gibbs energy curves of the binary systems LiF–BeF_2, LiF–ThF_4 (dashed line) and BeF_2–ThF_4, where the molar fraction corresponds to the amount of BeF_2, ThF_4 and ThF_4 again, at 1100 K.

BeF–ThF_4 mixtures could provide welcome information on the structure of the melt, because the model used here is not conclusive.

The shape of the diagram, calculated by the LiF asymmetry model, resembles the experimental diagram from Thoma et al. [8] much better than the BeF_2 asymmetry model and also the overall agreement with the experimental data is better. However, there is a feature when comparing the two models, which should be noted. Concerning the LiF asymmetry model, the lowest temperatures appear to have the largest deviation from the experimental values, which can be seen in Fig. 6, where the disagreement is slightly increasing with decreasing temperatures. This inevitably holds that the ternary invariant points, which belong to the lowest temperatures in the system, differ more from the experimental data than the liquidus at higher temperatures. A check was performed on the temperature dependence of the excess Gibbs energy. Therefore, a number of extra terms were introduced in the excess Gibbs energy function to see whether a better description could be obtained at the lower temperatures, but without satisfying result.

A similar plot comparing the model with the experiments was made for BeF_2 asymmetry as well, although it is not shown here. In this case, the deviations from the experimental data are larger and more scattered through the temperature spectrum. So, here it could happen that the invariant temperatures showed a better agreement with the experiments [7], but the compositions deviated more.

The miscibility gap present in LiF–BeF_2 has its influence on the ternaries LiF–BeF_2–ThF_4 and LiF–BeF_2–UF_4, where a small gap can be found close to the LiF–BeF_2 border at the BeF_2 rich part. However, the addition of exactly 1.0 mol% of ThF_4 and 0.9 mol% UF_4, which was revealed by systematically drawn pseudobinary diagrams crossing the ternary demixing areas, is enough to suppress this two-phase field. Hence it is explicable that Thoma et al. [8] and Jones et al. [9] do not mention the existence of ternary miscibility gaps.

Next to the miscibility gap, a couple of minor differences were found in the comparison with the invariant points of LiF–BeF_2–ThF_4, see Table 4, due to a change in the field stability of $LiF \cdot ThF_4$. Thoma et al. proposed the $LiF \cdot ThF_4$ phase to be stable in a small part of the diagram, ending in a peritectic at 0.63 LiF–0.30 BeF_2–0.07 ThF_4. In our model, this field is broader and ends in the peritectic at 0.34 LiF–0.65 BeF_2–0.01 ThF_4. A possible explanation could be the fact that four intermediate LiF–ThF_4 compounds exist of which we do not have thermodynamic data. They were optimized in the binary system, but it cannot be excluded that the description of the thermodynamic parameters is not sufficient for extrapolation in a ternary system.

Fig. 8 is an example of a pseudobinary cross-section through the LiF–BeF_2–ThF_4 diagram. It shows

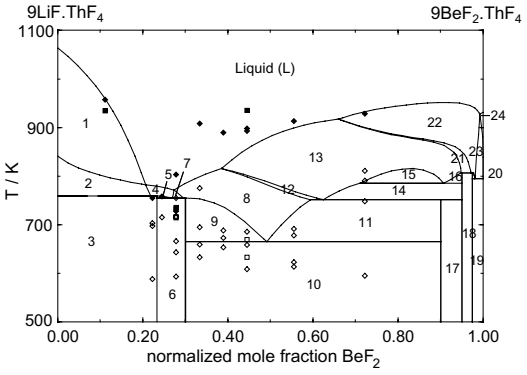

Fig. 8. Pseudobinary $Li_{0.9}Th_{0.1}F_{1.3}$–$Be_{0.9}Th_{0.1}F_{2.2}$ section of the pseudoternary LiF–BeF_2–ThF_4 system. (■) liquid, obtained by quenching; (◆) liquid, obtained by cooling; (□) other phase transitions obtained by quenching; (◇) other thermal effects occurring on cooling, all data extracted from tables according to Thoma et al. [8]. Phases: (1) LiF + L; (2) LiF + Li_3ThF_7 + L; (3) LiF + Li_3ThF_7 + Li_2BeF_4; (4) Li_3ThF_7 + L; (5) Li_3ThF_7 + Li_2BeF_4 + L; (6) Li_2BeF_4 + Li_3ThF_7 + $LiThF_5$; (7) Li_3ThF_7 + $LiThF_5$ + L; (8) $LiThF_5$ + L; (9) Li_2BeF_4 + $LiThF_5$ + L; (10) Li_2BeF_4 + $LiThF_5$ + BeF_2; (11) $LiThF_5$ + BeF_2 + L; (12) $LiThF_5$ + $LiTh_2F_9$ + L; (13) $LiTh_2F_9$ + L; (14) $LiTh_2F_9$ + BeF_2 + L; (15) $LiTh_2F_9$ + L + L_2; (16) $LiTh_2F_9$ + L; (17) $LiThF_5$ + $LiTh_2F_9$ + BeF_2; (18) $LiTh_2F_9$ + $LiTh_4F_{17}$ + BeF_2; (19) $LiTh_4F_{17}$ + ThF_4 + BeF_2; (20) $LiTh_4F_{17}$ + BeF_2 + L; (21) $LiTh_2F_9$ + $LiTh_4F_{17}$ + L; (22) $LiTh_4F_{17}$ + L, (23) $LiTh_4F_{17}$ + ThF_4 + L; (24) ThF_4 + L.

the complexity of the system, especially below the liquidus. It can be seen that the model reproduces the available liquidus data well, with the exception of the range $0.3 < X_{BeF_2} < 0.4$. Here the ORNL data show even an increase towards the eutectic, whereas the model decreases in temperature. Something else that should be noted is that the number of observed thermal effects observed in the ORNL experiments exceeds the number of calculated phase boundaries. It can be partly explained by the fact that one intermediate compound, $LiF \cdot BeF_2$, has deliberately been omitted from the assessment, since it decomposes in the solid phase and has no influence on the liquidus. But otherwise, it is interesting to have a closer examination of the range $0.2 < X_{BeF_2} < 0.4$ and to repeat the ORNL experiments to have more certainty which thermal signal corresponds to which phase transition. Generally, it would be helpful to know the intensity of the observed effects. We know from previous DTA measurements [19], that the formation of a eutectic or peritectic melt gives the sharpest signal, much more than when the liquidus is crossed, which is sometimes difficult to discern. One can wonder if the two observed liquidus signals at $X_{BeF_2} = 0.221$, $T = 754.9$ K and $X_{BeF_2} = 0.244$, $T = 758.5$ K are probably not misinterpreted eutectic and peritectic events? They coincide namely almost exactly with our calculated ternary invariant points of 758.9 K and 754.7 K, see Table 4.

In general it can be concluded that the polynomial model with Kohler–Toop extrapolation gives a satisfactory description of the binary and the higher order systems of $LiF–BeF_2–ThF_4–UF_4$, especially $LiF–BeF_2–UF_4$, $LiF–ThF_4–UF_4$ and $BeF_2–ThF_4–UF_4$, since the diagrams agree with the determined invariant points and the experimental liquidus data. Nevertheless, it might be worthwhile for a future study to use another model, for example the quasi-chemical model by Pelton et al. [20], to see if the agreement with experiments and model can be improved. For the system $LiF–NaF–LaF_3$ we made already a comparison between the results obtained by the quasi-chemical model and by the polynomial description we used in this study [19]. In that case it appeared that the differences are minor, but it is not certain what the results will be in $LiF–BeF_2–ThF_4–UF_4$.

4. Conclusion

$LiF–BeF_2–ThF_4–UF_4$ is the proposed fuel for the Molten Salt Reactor in the breeder design. Its ternary subsystems were calculated from the assessed Gibbs coefficients from the binary systems, which were obtained by using a general polynomial model, using an asymmetrical extrapolation that is based on the fact that one component of the ternary is chemically different from the other two. In case of the systems $LiF–BeF_2–ThF_4$ and $LiF–BeF_2–UF_4$, where the chemical asymmetry is more complicated, LiF was selected as the asymmetrical component, since its behavior is purely ionic in a melt, in contrary to the other fluorides. A good agreement with the experimental quenching and DTA cooling results on the ternaries from the literature was achieved.

As a result of a miscibility gap in $LiF–BeF_2$, a two-phase liquid region is present in $LiF–BeF_2–ThF_4$ and $LiF–BeF_2–UF_4$. However, it is very small in both systems and the addition of 1.0 mol% of ThF_4 and 0.9 mol% UF_4 is enough to suppress the two-phase liquid field.

The proposed composition for breeder fuel was 71.7% LiF–16% BeF_2–12% ThF_4–0.3% UF_4, with an experimentally determined melting point of 773 K. In our model, a fuel of this composition would melt at 794.5 K.

Overall it can be concluded that some targeted DTA experiments on ternary and quaternary compositions are required to check whether this difference can be ascribed to the way of interpretation of the cooling curves and quenching data by the Oak Ridge researchers. It is possible that a systematic shift exists between the events determined from the early experiments and those determined from our own DTA curves, implying that a re-interpretation according to our latest views could result in a better agreement between model and experiment. However, if the difference between model and experiments appears to be genuine, then we should reconsider the thermodynamic model used and change it or adapt it.

References

[1] E. Thilo, H.-A. Lehmann, Z. Anorg. Chem. 258 (1949) 332.
[2] D.M. Roy, R. Roy, E.F. Osborn, J. Am. Ceram. Soc. 33 (1950) 85.
[3] D.M. Roy, R. Roy, E.F. Osborn, J. Am. Ceram. Soc. 37 (1954) 300.
[4] A.V. Novoselova, Y.P. Simanov, E.I. Jarembash, Zh. Fiz. Khim. SSSR 26 (1952) 1244.
[5] R.E. Thoma, H. Insley, H.A. Friedman, G.M. Hebert, J. Nucl. Mater. 27 (1968) 166.
[6] K.A. Romberger, J. Braunstein, R.E. Thoma, J. Phys. Chem. 76 (1972) 1154.

[7] J.P.M. van der Meer, R.J.M. Konings, M.H.G. Jacobs, H.A.J. Oonk, J. Nucl. Mater. 344 (2005) 94.
[8] R.E. Thoma, H. Insley, H.A. Friedman, C.F. Weaver, J. Phys. Chem. 64 (1960) 865.
[9] L.V. Jones, D.E. Etter, C.R. Hudgens, A.A. Huffman, T.B. Rhinehammer, N.E. Rogers, P.A. Tucker, L. Wittenberg, J. Am. Ceram. Soc. 45 (1962) 79.
[10] C.F. Weaver, R.E. Thoma, H. Insley, H.A. Friedman, J. Am. Ceram. Soc. 43 (1960) 214.
[11] C.F. Weaver, R.E. Thoma, H.A. Friedman, G.M. Hebert, J. Am. Ceram. Soc. 44 (1961) 146.
[12] M.W. Chase Jr. (Ed.), NIST-JANAF Thermochemical Tables, 4th Ed., J. Phys. Chem. Ref. Data Monograph 9.
[13] R.J.M. Konings, J.P.M. van der Meer, E. Walle, Chemical Aspects of Molten Salt Reactor Fuel, Tech. Rep. JRC-ITU-TN 2005/25, 2005.
[14] C.W. Bale, P. Chartrand, S.A. Degterov, G. Eriksson, K. Hack, R. BenMahfoud, J. Melançon, A.D. Pelton, S. Petersen, CALPHAD 62 (2002) 189.
[15] A.D. Pelton, M. Blander, Metall. Trans. 17B (1986) 805.
[16] W.R. Grimes, Nucl. Appl. Tech. 8 (1970) 137.
[17] S. Cantor, J.W. Cooke, A.S. Dworkin, G.D. Robbins, R.E. Thoma, G.M. Watson, Tech. Rep. Report ORNL-TM-2316, 1968.
[18] F. Vaslov, A.H. Narten, J. Chem. Phys. 59 (1973) 4949.
[19] J.P.M. van der Meer, R.J.M. Konings, K. Hack, H.A.J. Oonk, Chem. Mater. 18 (2005) 510.
[20] A.D. Pelton, P. Chartrand, G. Eriksson, Metall. Trans. 32A (2001) 1409.
[21] R.E. Thoma, H. Insley, B.S. Landau, H.A. Friedman, W.R. Grimes, J. Phys. Chem. 63 (1959) 1266.
[22] C.J. Barton, H.A. Friedman, W.R. Grimes, H. Insley, R.E. Moore, R.E. Thoma, J. Am. Ceram. Soc. 41 (1958) 63.